

Finger patterns produced by thermomagnetic instability in superconductors

A. L. Rakhmanov¹, D. V. Shantsev^{2,3}, Y. M. Galperin^{2,3}, T. H. Johansen^{2,4,*}

¹ *Institute for Theoretical and Applied Electrodynamics, Izhorskaya 13/19, Moscow, 125412, Russia*

² *Department of Physics, University of Oslo, P. O. Box 1048 Blindern, 0316 Oslo, Norway*

³ *A. F. Ioffe Physico-Technical Institute, Polytekhnicheskaya 26, St. Petersburg 194021, Russia*

⁴ *Texas Center for Superconductivity and Advanced Materials,
University of Houston, Houston Texas, 77204-5002 USA*

(Dated: October 2, 2018)

A linear analysis of thermal diffusion and Maxwell equations is applied to study the thermomagnetic instability in a type-II superconducting slab. It is shown that the instability can lead to formation of spatially nonuniform distributions of magnetic field and temperature. The distributions acquire a finger structure with fingers perpendicular to the screening current direction. We derive the criterion for the instability, and estimate its build-up time and characteristic finger width. The fingering instability emerges when the background electric field is larger than a threshold field, $E > E_c$, and the applied magnetic field exceeds a value $H_{\text{fing}} \propto 1/\sqrt{E}$. Numerical simulations support the analytical results, and allow to follow the development of the fingering instability beyond the linear regime. The fingering instability may be responsible for the nucleation of dendritic flux patterns observed in superconducting films using magneto-optical imaging.

I. INTRODUCTION

The thermomagnetic instability or flux jumping is commonly observed at low temperatures in type-II superconductors with strong pinning.¹⁻⁴ The instability arises because of two fundamental reasons: (i) motion of magnetic flux releases energy, and hence increases the local temperature; (ii) the temperature rise decreases flux pinning, and hence facilitates the flux motion. This positive feedback can result in thermal runaways and global flux redistributions jeopardizing superconducting devices. This mechanism was understood in early works,^{5,6} and later on the thermomagnetic instability was studied thoroughly (see Refs. 1-4 for a review). In particular, the threshold magnetic field for the instability was calculated and its experimentally found dependence on temperature, sample dimensions, and the applied field ramping rate were explained.

The conventional theory of the thermomagnetic instability^{1,2} predicts “uniform” flux jumps, where the flux front is essentially flat. In other words, the spatial extension of the instability region tends to be maximal since small-scale perturbations are stabilized by thermal diffusion. This picture is true for many experimental conditions, however, not for all. Numerous magneto-optical studies have revealed that the thermomagnetic instability in thin superconducting samples results in dendritic flux patterns.⁷⁻¹⁸ In course of the dendritic instability the flux forms narrow “fingers” of typical width 20–50 μm and length up to the size of the sample. Such a behavior clearly contradicts to the conventional theoretical concepts and needs elucidation.

Few attempts to describe a nonuniform development of the thermomagnetic instability have been made. Among them is a numerical solution of thermal diffusion and Maxwell equations that can result in a rather nonuniform temperature distribution for a bulk superconductor.¹⁹ Molecular dynamics simulations of flux quanta motion in

superconducting film¹³ can model dendritic flux and temperature patterns similar to those found experimentally. However, these numerical results still lack analytical support. In particular, it is still unclear what kind of spatial structure can be formed during a flux jump, and under what conditions. A similar problem was analyzed in a recent work²⁰ where the propagating flux front was shown to acquire a non-uniform spatial structure if its speed is higher than some critical value, and the conductivity is a strong function of flux density. In the present study it is shown that these assumptions are not necessary requirements for a superconductor to develop nonuniform flux jumps.

In the present paper the spatial pattern of the instability in a bulk superconductor is studied using the conventional approach^{1,2,5} – linear analysis of a set of differential equations describing small perturbations in the electric field E and temperature T . In contrast to the previous investigations, we allow the perturbations to vary in any direction, i. e., both parallel and perpendicular to the direction of the background current \mathbf{j} and field \mathbf{E} . In this way we determine the stability criteria and also estimate the instability build-up time. As a main result we find that the most unstable perturbations are in the form of narrow fingers perpendicular to the background field \mathbf{E} and occur if E is larger than some threshold value. This shape prevents current adjustment across the perturbed region and, hence, yields the fastest perturbation growth. Too narrow fingers are, however, suppressed by the thermal diffusion. Thus, the typical finger size, $\sqrt{\kappa(\partial j_c/\partial T)^{-1}/E}$, where κ is the thermal conductivity and j_c is the critical current density, is determined by the competition between the Joule heat jE and thermal diffusion, $\kappa\nabla^2 T$.

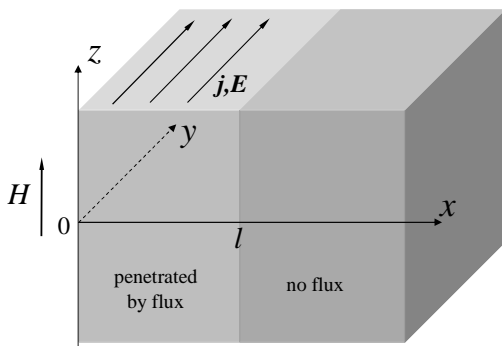


FIG. 1: Superconductor geometry.

II. BASIC EQUATIONS

We shall study the instability in the simplest geometry, i. e., in a superconducting slab placed in a parallel magnetic field, see Fig. 1. The slab fills the semispace $x > 0$, and the external magnetic field \mathbf{H} is parallel to the z -axis so that the screening current \mathbf{j} flows along the y -axis. The current and magnetic field distributions in the sample are determined by the Maxwell equation, with a proper boundary condition

$$\text{curl } \mathbf{B} = \mu_0 \mathbf{j}, \quad \mathbf{B}|_{x=0} = \mu_0 \mathbf{H}. \quad (1)$$

Here the local magnetic field in the flux penetrated part of the slab is assumed larger than the first critical field, and hence, to a good approximation $B(x, y) = \mu_0 H(x, y)$. To find the temperature and electric field in a superconductor the corresponding thermal and the second Maxwell equations should be used:

$$C(\partial T / \partial t) = \kappa \nabla^2 T + \mathbf{j} \mathbf{E}, \quad (2)$$

$$\text{curl } \mathbf{E} = -\partial \mathbf{B} / \partial t, \quad (3)$$

where C is the specific heat.

These equations should be supplemented by a current-voltage curve $j = j(E, B, T)$. In type-II superconductors the $j(E)$ dependence is strongly nonlinear. As a result, a quasi-static critical state with $j \approx j_c(B, T)$ is formed. This will be the initial state from which the instability evolves. For simplicity we use the Bean model, i. e. we neglect any B dependence of the critical current density j_c . The exact form of the current-voltage curve,

$$\mathbf{j} = j(T, E) (\mathbf{E} / E). \quad (4)$$

is not crucially important. The only important point is that the $E(j)$ curve is very steep, and therefore its logarithmic derivative is large:

$$n(E) \equiv \frac{\partial \ln E}{\partial \ln j} \approx \frac{j_c}{\sigma E} \gg 1. \quad (5)$$

Here σ is the differential conductivity,

$$\sigma(E) \equiv \partial j / \partial E. \quad (6)$$

At low electric fields, the $E(j)$ curve is often approximated by a power law, i. e., n is assumed independent of E , and $E \propto j^n$. Our approach is applicable also to the flux flow regime at high electric fields. In that regime $\sigma(E) = \sigma_f$ is the flux-flow Ohmic conductivity and $n(E) = j_c / \sigma_f E \propto 1/E$.

The key dimensionless parameter of the model is the ratio of thermal and magnetic diffusion coefficients:

$$\tau \equiv \mu_0 \sigma \kappa / C. \quad (7)$$

The smaller τ is, the slower heat diffuses from the perturbation region into the surrounding areas. Hence, one can expect that for smaller τ ; (i) the superconductor is more unstable, and (ii) the formation of instability-induced nonuniform structures is more favorable.

III. PERTURBATION ANALYSIS

A. Linearization of the problem

We seek solutions of the equations presented above in the form,

$$T + \delta T(x, y, t), \quad \mathbf{E} + \delta \mathbf{E}(x, y, t), \quad (8)$$

where T and \mathbf{E} are the background values. The background field \mathbf{E} may be created by ramping the external magnetic field H , or by other sources as discussed in Sec. VI. In practice \mathbf{E} is nonuniform, but for simplicity we disregard its coordinate dependence. For a weak non-uniformity that can be justified using the method of Ref. 21, based on Wentzel-Kramers-Brillouin approximation. In this approximation the non-uniformity results only in replacement some of local quantities by the ones averaged over x . Hence, we get only insignificant numerical corrections. Numerical simulations in Sec. V show that this conclusion also holds in the realistic situation when the non-uniformity of \mathbf{E} is induced by the by ramping the external magnetic field H . Similarly, we ignore any coordinate dependence of the background temperature. This can be done if it satisfies the inequality $T(x, y) - \bar{T} \ll T_c - \bar{T}$, where T_c is the critical temperature of the superconductor, and \bar{T} is the sample-averaged temperature before the instability build-up.

From the symmetry of the problem $E_x = 0$, while for the perturbation $\delta \mathbf{E}$ both δE_x and δE_y in general do not vanish. The linearization of the $E(j)$ in (4) yields

$$\delta \mathbf{j} = \left(\frac{\partial j_c}{\partial T} \delta T + \sigma \delta E \right) \frac{\mathbf{E}}{E} + j_c \left(\frac{\delta \mathbf{E}}{E} - \delta E \frac{\mathbf{E}}{E^2} \right). \quad (9)$$

Since the vector \mathbf{E} is parallel to the y -axis, one has in the linear approximation that $\delta E = \delta E_y$, and as a result one finds

$$\delta \mathbf{j} = \left(\frac{\partial j_c}{\partial T} \delta T + \sigma \delta E_y \right) \frac{\mathbf{E}}{E} + j_c \frac{\delta \mathbf{E}_x}{E}. \quad (10)$$

We shall seek perturbations in the usual form:

$$\delta T = T^* \theta \exp(\lambda t/t_0 + ik_y \eta + ik_x \xi), \quad (11)$$

$$\delta E_{x,y} = E \varepsilon_{x,y} \exp(\lambda t/t_0 + ik_y \eta + ik_x \xi), \quad (12)$$

where $\xi = x/w$, $\eta = y/w$, and

$$\frac{1}{T^*} = -\frac{1}{j_c} \frac{\partial j_c}{\partial T}, \quad t_0 = \frac{\sigma C T^*}{j_c^2} = \mu_0 \sigma w^2, \quad w^2 = \frac{C T^*}{\mu_0 j_c^2}.$$

Here θ and $\varepsilon_{x,y}$ are the Fourier amplitudes, $\text{Re } \lambda$ is the dimensionless instability increment, t_0 is the characteristic time of adiabatic heating, which coincides with the magnetic diffusion time for the length w , and w is the characteristic scale for the adiabatic instability.¹ The wave numbers k_y and k_x characterize the scale of the perturbation along the y and x axes, respectively. Since the sample is assumed infinite in the y direction, the k_y is arbitrary, while k_x is determined by the width of the flux penetrated region and the corresponding boundary conditions.

Let us define the Fourier amplitude of the dimensionless current perturbation $\delta \mathbf{j}/j_c$ as \mathbf{i} . Using Eqs. (10)–(12) one finds the components of the vector \mathbf{i} in the form

$$i_x = \varepsilon_x, \quad i_y = -\theta + \varepsilon_y/n. \quad (13)$$

Using Eq. (2) one obtains the equation for the temperature perturbation θ as

$$\lambda \theta = -\tau(k_y^2 + k_x^2)\theta + (i_y + \varepsilon_y)/n. \quad (14)$$

We find from Eq. (14)

$$\theta = \frac{(1 + 1/n)\varepsilon_y}{n\lambda + n\tau(k_y^2 + k_x^2) + 1}. \quad (15)$$

Then, using Eqs. (1) and (3), we can rewrite the Maxwell equation for the perturbation as

$$\mathbf{k} \times [\mathbf{k} \times \vec{\varepsilon}] = \lambda n \mathbf{i}. \quad (16)$$

Using the relations (13) we cast Eq. (16) into the equation set for dimensionless components of the electric field perturbation

$$\varepsilon_x = \frac{k_y k_x}{k_y^2 + \lambda n} \varepsilon_y, \quad (17)$$

$$-k_x^2 \varepsilon_y + k_y k_x \varepsilon_x = \lambda n (-\theta + \varepsilon_y/n). \quad (18)$$

Note that these equations together with Eqs. (13) and (15) provide continuity of the current perturbation, i. e., $\text{div } \delta \mathbf{j} = 0$, as required. Substituting Eqs. (15) and (17) in Eq. (18) one finds the following dispersion equation providing nontrivial solutions for ε_y :

$$\frac{1 - \lambda - \tau(k_y^2 + k_x^2)}{n\lambda + n\tau(k_y^2 + k_x^2) + 1} = \frac{k_x^2}{k_y^2 + n\lambda}. \quad (19)$$

The corresponding quadratic equation for $\lambda(k_x, k_y)$ has the form

$$\lambda^2 + P\lambda + Q = 0, \quad (20)$$

where

$$P = k_x^2 + k_y^2/n - 1 + \tau(k_y^2 + k_x^2),$$

$$Q = \frac{k_x^2 - k_y^2}{n} + \tau \left(k_x^4 + \frac{n+1}{n} k_x^2 k_y^2 + \frac{1}{n} k_y^4 \right). \quad (21)$$

The system is unstable if $\text{Re } \lambda(k_x, k_y) > 0$.

B. Qualitative Analysis

The dispersion equation becomes more transparent when the heat conductivity can be neglected, i. e. $\tau = 0$. Then,

$$\lambda^2 + \lambda(k_x^2 + k_y^2/n - 1) + (k_x^2 - k_y^2)/n = 0. \quad (22)$$

First, we notice that at $k_x = 0$ the system is always unstable. This is not surprising since such solutions correspond to the case of a sample with fixed transport current, $i_y = 0$, heated by the electric field E under adiabatic conditions. In this case δE and δT grow with the maximal possible rate, $\lambda = 1$, and the characteristic time of the instability build-up is t_0 .

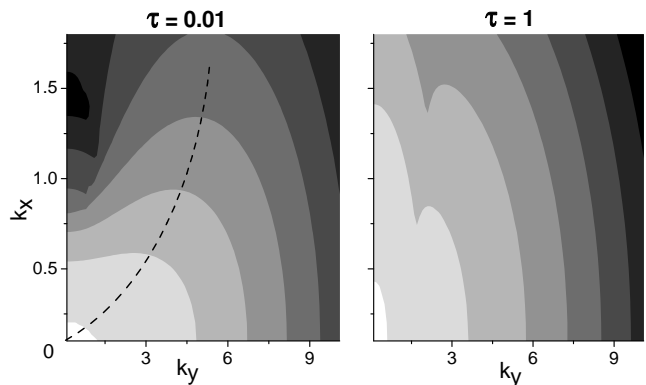


FIG. 2: The contour plots for the instability increment $\text{Re } \lambda(k_x, k_y)$ obtained from Eq. (20) for $n = 10$. The brightest areas correspond to the fastest growth of instability. For low τ perturbations with a finite k_y have the maximal increment, while for large τ (strong heat diffusion), uniform perturbations with $k_y = 0$ would grow fastest.

For a finite sample the k_x is not arbitrary because of the boundary conditions at the edges of the flux penetrated region. Only some particular k_x satisfy the boundary conditions, which makes the system more stable. For example, for perturbations uniform in the y -direction ($k_y = 0$) the instability develops only if $k_x < 1$. However, if we set $k_y \rightarrow \infty$, then the system becomes unstable for

any k_x , and we again arrive at the maximal growth rate, $\lambda = 1$. This result can be understood physically, if we take into account that infinite k_y correspond to a perturbation in the form of a narrow finger directed along the y axis, i. e., perpendicular to the current flow. The current flow remains unperturbed by an infinitesimally narrow finger i. e., the condition $i_y = 0$ least favorable for the stability holds, like for the case $k_x = 0$. In the case of wider fingers, the current adjusts itself to the temperature fluctuation, which slows down the instability growth. So, if one neglects the thermal diffusion, the narrowest possible fingers are the most favorable ($k_y \rightarrow \infty$), and the superconducting state is utterly unstable.

The thermal diffusion evidently suppresses the instability growth. The suppression is most effective for large k_y . As a result, we obtain some optimal value of k_y , for which the instability increment λ is maximal. The existence of such an optimal k_y is evident from the contour plot of $\text{Re } \lambda$ calculated for $\tau = 0.01$, see Fig. 2, left. The dashed line shows k_y providing the maximal $\text{Re } \lambda$ for a given k_x . However, if τ is larger then the heat diffusion fully dominates the instability development. In that case the maximal λ corresponds to $k_y = 0$, see Fig. 2, right.

IV. RESULTS

In this section we solve the problem more accurately, and start by establishing the proper boundary conditions.

A. Boundary conditions

From the above analysis it is clear that a finger structure may appear only for $\tau < 1$. Consequently, we focus only on this case. Since the thermal diffusion is then slower than the magnetic diffusion, we can impose only the electrodynamic boundary conditions. This is equivalent to neglecting the heat flux in the x direction, i. e., the term τk_x^2 in Eq. (14) can be omitted.

The magnetic field at the slab surface is equal to the applied field, hence the perturbation at the surface is zero, $\delta h_z = 0$ at $x = 0$. The magnetic field has only z -component, thus from Eqs.(3) and (17) one obtains $\delta E'_y \propto \delta h_z$, and the first boundary condition is

$$\delta E'_y = 0, \quad x = 0. \quad (23)$$

This condition also means that the current does not flow across the sample surface, $\delta j_x \propto \delta E_x = 0$ at $x = 0$.

Let us specify the boundary conditions at the flux front, $x = l$. In the flux-free region, $x > l$, the electric field decays on the scale of the London penetration depth, which is much smaller than any spatial scale of the problem. Therefore, the continuity of the tangential component of the electric field requires,

$$\delta E_y = 0, \quad x = l. \quad (24)$$

These boundary conditions together with Eqs. (13), (14) and (16) are satisfied when $\delta E_y \propto \cos(k_x x/w)$ with

$$k_x = (\pi/2)(w/l).$$

Now we can search for solutions of Eq. (20) with this k_x , and as before, when $\text{Re } \lambda > 0$ the system is unstable.

B. Instability criterion and increment

Let first consider the spatially uniform case where there exists a well-known criterion for the thermomagnetic stability.¹⁻⁶ With $k_y = 0$ and using $\tau \ll 1$, i. e. for very slow thermal diffusion we find from Eq. (20) that the system is unstable if $k_x < 1$. For the Bean model, where $l = H/j_c$, this is expressed as

$$H > H_{\text{adiab}} = (\pi/2)\sqrt{CT^*/\mu_0}, \quad (25)$$

which is the commonly used adiabatic criterion for flux jumps.

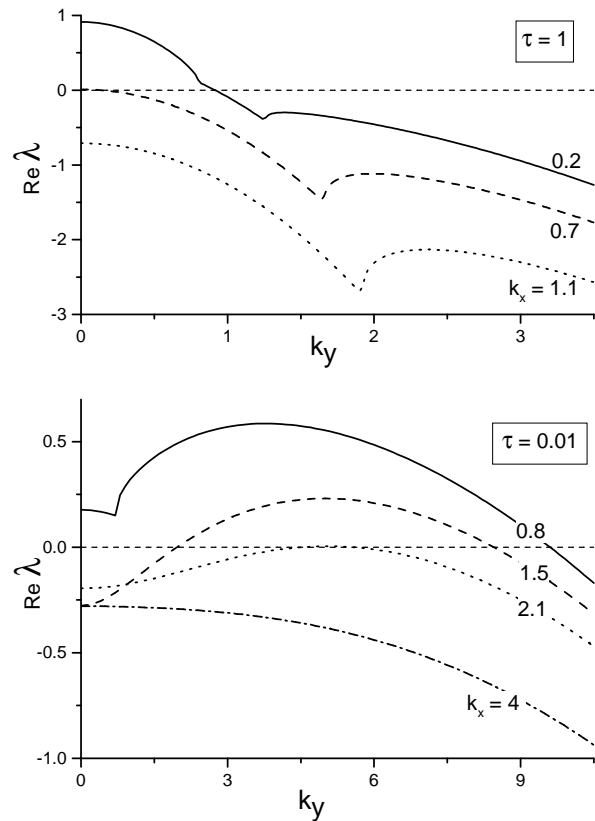


FIG. 3: The instability increment $\text{Re } \lambda(k_y)$ found from Eq. (20) for $n = 10$ and different k_x . Top: fast heat diffusion, the maximal increment corresponds to uniform perturbations ($k_y = 0$). Bottom: slow heat diffusion, the maximal $\text{Re } \lambda$ is found at a finite k_y .

Let us next consider cases of non-zero k_y , and analyze the behavior of $\text{Re } \lambda(k_y)$. Shown in Fig. 3 (top) are

plots for $\tau = 1$. For small applied magnetic fields the system is stable, see the curve for $k_x = 1.1$. As the field increases, the flux penetration depth grows, and hence k_x goes down. For $k_x = 0.7$ the system becomes unstable, i. e., solutions with $\text{Re } \lambda > 0$ arise. Note that the instability appears first at $k_y = 0$. For higher fields ($k_x = 0.2$), the instability range extends to large k_y too, but the maximal $\text{Re } \lambda$ always corresponds to $k_y = 0$.²² Therefore, for relatively large τ the instability develops in a uniform mode.

However, for smaller τ the $\text{Re } \lambda(k_y)$ behaves differently, see Fig. 3 (bottom). The maximal $\text{Re } \lambda$ can here occur for a non-zero k_y . Moreover, it is possible that the system is stable with respect to uniform perturbations, while unstable for perturbations with finite k_y , see the curve for $k_x = 1.5$. This means that a non-uniform structure along the y -direction will be formed.

When the applied magnetic field gradually increases from zero, the instability first starts for some particular $k_x = k_x^*$ when $\text{Re } \lambda = 0$ only for one single value of $k_y = k_y^*$. This is the case for $k_x = k_x^* = 2.1$ in Fig. 3 (bottom). To find these k_y^* and k_x^* one needs two conditions. The first one is

$$Q(k_x^*, k_y^*) = 0, \quad (26)$$

which is a quadratic equation with respect to $(k_y^*)^2$, and the second one is that the discriminant of this equation is zero. Using Eq. (21) and the fact that $n \gg 1$, we find

$$k_y^* = \left(\frac{2}{n}\right)^{1/4} \frac{1}{\sqrt{\tau}}, \quad k_x^* = \frac{1}{\sqrt{n\tau}}, \quad (27)$$

The instability occurs at $k_x < k_x^*$, and for large n this instability criterion can be written as

$$E > (\pi^2/4) (\kappa T^*/j_c l^2). \quad (28)$$

One can see from Fig. 3 (bottom) that the value of k_y where $\text{Re } \lambda$ has the maximum depends only weakly on k_x . Therefore, a good estimate for the finger width d_y in the y direction is w/k_y^* . Thus

$$d_y \approx \left(\frac{\kappa}{E \partial j_c / \partial T}\right)^{1/2} \frac{1}{(2n)^{1/4}}. \quad (29)$$

Once we go from the instability threshold towards lower k_x , the increment $\text{Re } \lambda$ quickly becomes of the order of unity. Thus, the characteristic time of the instability development is of the order of the adiabatic time, t_0 .

The aspect ratio of the perturbed region is

$$k_y^*/k_x^* \approx (2n)^{1/4}. \quad (30)$$

Note that it is independent of the thermal parameters, C, κ, T^* , and determined only by the shape of the $E(j)$ curve.

As was seen from Fig. 3, the instability will develop uniformly for $\tau = 1$, and non-uniformly for $\tau = 0.01$.

It follows directly that the border between the uniform and non-uniform regimes is given by the criterion $\text{Re } \lambda(k_x^*, k_y = 0) = 0$. Using Eqs. (20) and (27) one can rewrite the criterion as $\tau = 1/n$. Rewriting this in dimensional form we conclude that for

$$E > E_c = \mu_0 \kappa j_c / C \quad (31)$$

the instability will evolve non-uniformly.

V. SIMULATIONS

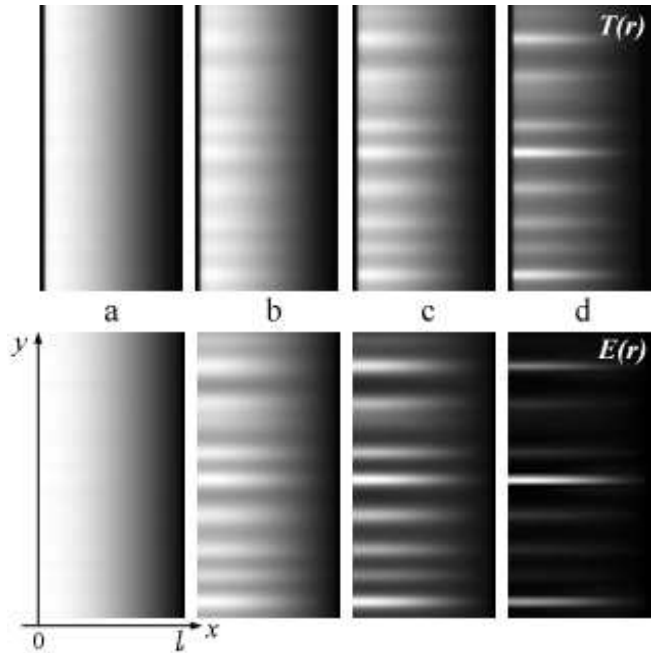


FIG. 4: Evolution of the temperature T and electric field E_y distributions produced by simulations that illustrate the formation of a finger structure. The instability was triggered by a uniform electric field, $E_y = E_0$, switched on at $t = 0$. The images (a–d) correspond to the times $t/t_0 = 1.6, 3.0, 3.2$, and 3.3 , respectively.

In order to visually illustrate the formation of non-uniform structures, and to verify the validity of the above analytical results, numerical simulations based on the Maxwell and thermal diffusion equations Eqs. (1), (2) and (3) were carried out. In the simulations we went beyond the linear approximation and considered the full non-linear $E(j)$ curve, which was chosen to be

$$E = \frac{j}{\sigma_f + (j_c/j)^{\tilde{n}-1} j_{c0}/E_0}, \quad (32)$$

where j_{c0} and E_0 are constants. This is one of possible smooth interpolations between the flux creep regime at small currents with $E \propto j^{\tilde{n}}$, and the Ohmic flux flow regime $E = j/\sigma_f$ at high j . Here the flux flow resistivity is much higher than the characteristic resistivity in the

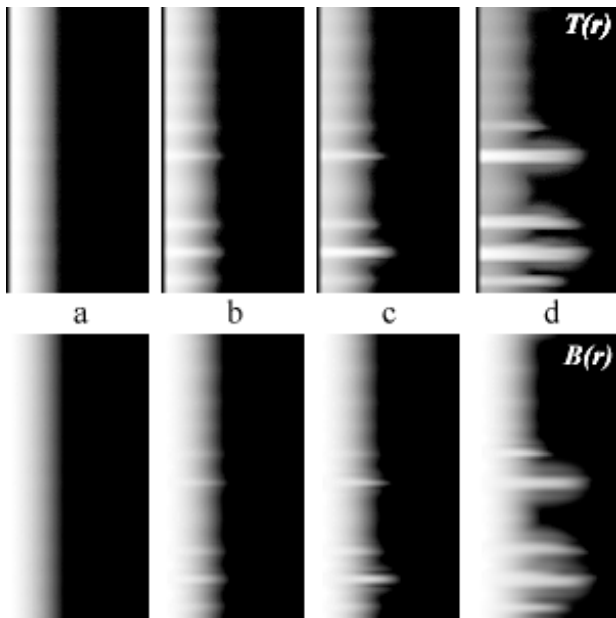


FIG. 5: Evolution of the temperature and flux density distributions produced by simulations. The instability is triggered by applying a magnetic field. The images (a-d) correspond to the times $t/t_0 = 45, 46.1, 46.15,$ and $46.25,$ respectively. The formation of fingers and their propagation into the flux free area is clearly seen.

flux creep regime, $\sigma_f^{-1} = 10^4 E_0 / j_{c0}$. The temperature dependence of the critical current density is assumed to be linear, $j_c = j_{c0} [1 - (T - T_0) / T^*]$. The electrodynamic boundary conditions are $dE_y/dx(x=0) = 0$ (constant external magnetic field), $E_y(x=l) = 0$, $E_x(x=0, l) = 0$, with $l = 2w$, and the periodic boundary conditions in the y direction. Since the thermal boundary conditions are not of crucial importance at $\tau \ll 1$, we used the simplest ones, $T(x=0) = T_0$ (ideal heat removal at the surface) and $dT/dx(x=l) = 0$ (the symmetry condition in the middle of the slab).

Our analytical results predict that the instability will form a finger structure if a sufficiently large uniform background electric field is present. Therefore, for initial conditions we assume a uniform electric field, $E_y(0 \leq x < l, t=0) = E_0$. To introduce some non-uniformity into the system small random values $\delta T_R \ll T^*$ were added to the initial temperature for every discrete node. The initial temperature is then given as $T(x, t=0) = T_0 + \delta T_R$. The key parameters $\tau = 0.001$ and $n \approx \tilde{n} = 30$ are specified at $E = E_0$. Their dependences on the electrical field are given by Eqs. (5), (6) and (32). Since now $E_0 = E_c / (n\tau) \gg E_c$, the condition (31) is fulfilled, and the instability is expected to develop in a non-uniform fashion. This is indeed confirmed by the calculated evolution of E_y and T distributions presented in Fig. 4. The numerical solution was performed on a grid of 140×70 nodes using a simple-step integration method.

One can see from Fig. 4(a) that at small times the distributions of E and T are essentially uniform along the y axis. Then, a finger structure is emerging (b) with protrusions perpendicular to the electric field direction, as predicted by our previous linear analysis. The simulations also show how this finger structure is evolving beyond the linear regime. We can see that the electrical field in some fingers grows faster so that relative difference between the fingers increases (c). Eventually, the most intense finger takes over and dominates the entire E distribution (d). We believe that the reason for such behavior is the increase of the differential resistivity as E grows, Eq. (32). The growth of E is significant: the average value $\bar{E}_y = 1.7E_0$ for (a), and $21E_0$ for (d). Note that this growth cannot be traced from the presented images only because the gray scale was optimized for each individual image to provide the best contrast. More detailed simulations showed that the instability growth slows down only when the increasing E reaches the inflection point on the $E(j)$ curve before entering the flux flow regime.

Next, we carry out simulations with different initial and boundary conditions. We start from zero electric field, $E(t=0) = 0$, and assume that a linearly increasing magnetic field is applied to the slab so that $-dE_y/dx = dH/dt = 0.03w j_c / t_0$ at $x=0$. The other parameters are the same except that now the slab halfwidth is $6w$. The right edge of the distributions shown in Fig. 5 corresponds to the middle of the slab. One can see from Fig. 5(a) that for small H the flux penetrates in the conventional way, and a Bean-like profile of flux density is gradually advancing into the slab. When H and correspondingly E increase further, an instability sets in and leads to the formation of fingers (b-d). The finger structure is apparent in both the B and T distributions, especially on the later stages when only few intense fingers remain. Remarkably, the fingers tend to propagate into the flux free region, strongly distorting the flux front (d). One can speculate that these growing fingers eventually will develop into a complex dendritic flux pattern observed by magneto-optical imaging.⁷⁻¹⁸

The instability criteria and its growth rate found from the simulations are in a good agreement with our analytical results. Moreover, the simulations demonstrate that the finger instability arises even if some assumptions made in the derivation are relaxed. In particular, one does not necessarily need a strictly uniform background E and T distributions as assumed in the derivation. Furthermore, the background E and T distributions can also be non-stationary, which is always the case in a real experiment. In fact, in the simulations relevant to Fig. 5, where the instability was triggered by increasing the applied magnetic field, the E and T distributions were non-uniform and non-stationary. The formation of finger structure also turned out to be rather insensitive to the boundary conditions. We have also carried out simulations assuming that j_c in Eq. (32) depends on the local B according to the Kim model,²³ $j_c(B) \propto (B_0 + |B|)^{-1}$.

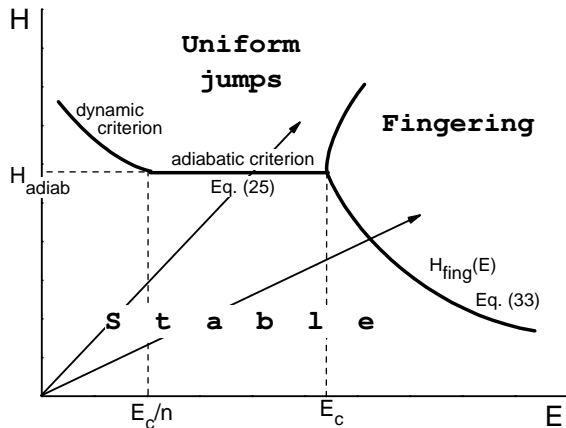


FIG. 6: Instability phase diagram in the plane magnetic field – electric field. The horizontal line corresponds to the adiabatic criterion for uniform jumps, Eq. (25). For $E > E_c$, the instability has a finger structure, and the criterion is given by Eq. (33).

With $B_0 = 3\mu_0 w j_c(0)$ we found similar distributions, thus proving that the finger instability can arise also in cases with a B dependent $E(j)$.

The simulations presented here have some similarities with those by Aranson *et al.*¹⁹ The main differences are that Aranson *et al.* started from a fully-penetrated state, the instability was nucleated by a local heat pulse, and j_c was generally nonuniform. As a result, the obtained patterns of T distribution look different from ours. Nevertheless, they also found that the instability results in a non-uniform T distribution only at small τ .

VI. DISCUSSION

The results obtained in this work can be graphically summarized by the instability “phase diagram” shown in Fig. 6. For small electric fields, $E < E_c$, the conventional uniform instability is favorable, and the adiabatic instability criterion Eq. (25) is applicable. For $E > E_c$ the fingering instability develops, with the instability criterion given by Eq. (28). Using the Bean model, $H = j_c l$, we obtain the finger instability criterion as

$$H > H_{\text{fing}} = (\pi/2)\sqrt{\kappa T^* j_c / E}, \quad E > E_c. \quad (33)$$

Figure also shows the border between the regions of uniform jumps and fingering instability for $H > H_{\text{adiab}}$ that was calculated from Eq. (20) using two conditions, $\partial \text{Re } \lambda / \partial k_y|_{k_y=k_0} = 0$, and $\text{Re } \lambda(k_x, k_0) = \text{Re } \lambda(k_x, 0)$.

Strictly speaking our analysis applies to the case $\tau < 1$, which is equivalent to $E > E_c/n$. For smaller electric fields a similar stability analysis can be made, taking into account the heat flux along the x axis. As expected, we found that for $E < E_c/n$ the uniform development of instability is always preferable. The instability criterion is

given by the well-known dynamic criterion, that is highly sensitive to the external cooling conditions.^{1,2} However, in all cases the flux jump field decreases monotonously with E , as indicated schematically in Fig. 6.

The finger instability occurs only at rather large background electric field. This field can be created by different sources. For example, if the applied magnetic field increases with a rate \dot{H} , an electric field $E \sim \dot{H}l \sim \dot{H}H/j_c$ is generated. Thus, when increasing H with a constant rate we move in the phase diagram in Fig. 6 along a straight line starting from the origin. For small \dot{H} , one crosses the instability boundary at $E < E_c$, resulting in a uniform flux jump. For large \dot{H} , the stability is destroyed for smaller H , and results in the formation of a non-uniform spatial structure. The predicted downturn of the $H(E)$ instability line at large E can be checked experimentally.

Numerical estimates were made using typical parameters for low-temperature superconductors at helium temperatures: $j_c = 10^{10}$ A/m², $C = 10^3$ J/Km³, $T^* = 10$ K, $\kappa = 10^{-2}$ W/Km, and $n = 30$. We then find the following values for the characteristic fields, $H_{\text{adiab}} \approx 0.1$ T, and $E_c \approx 0.1$ V/m, a finger width of $d_y \approx 3 \mu\text{m}$ for $E \sim E_c$, and a build-up time of the instability, t_0 , in the μs range. These estimates are not far from those reported in experimental papers, namely dendritic fingers of width 20-50 μm ,^{8,11,14,16} and the instability build-up time of $\sim 0.1 \mu\text{s}$.⁸⁻¹⁰ The criterion for the fingering instability $E > E_c$ can also be written down as $\sigma < \sigma_c = C/n\mu_0\kappa$. Using the numbers above we find $\sigma_c = 3 \times 10^9 \Omega^{-1}\text{m}^{-1}$, which is a reasonable value for the flux-flow conductivity. Correspondingly, for $\sigma = \sigma_c$ one obtains $\tau = 1/n \sim 1/30$.

Note that the electric field, E_c , needed for the finger instability to occur is not very small. As an estimate, the magnetic field ramp rate $\mu_0\dot{H}$ that induces the electric field E_c is of the order of 10^2 T/s for $l=1$ mm. Rates of similar magnitude are conventionally used for pulsed magnetization of superconducting permanent magnets.^{24,25} In experiments reporting the fingering instability⁷⁻¹⁸ the ramp rates were much smaller. One should keep in mind however that the actual electric field can be much larger than it follows from the simple estimate $\mu_0\dot{H}l$. The reason is a strong non-uniformity of the flux penetration both in space and in time, see for review Ref. 26. Hence, one can expect rather large local electric fields that last longer than the inverse instability increment, $\gtrsim 1 \mu\text{s}$. Other sources of large electric fields include random fluctuations of the superconductor parameters due to, e. g., relaxation of mechanical stresses. A very large electric field can be also created on purpose, e. g., by a laser pulse, which nucleates highly nonuniform flux distributions.⁸⁻¹⁰

In any case, it is rather difficult to meet the fingering instability criterion, $E > E_c$. This might be the reason why fingering is hardly observed in bulk samples. We are aware of only one experimental work⁷ where an indication of the discussed fingering instability in relatively

thick samples (with thickness up to 2 mm) was obtained. Another possible reason for why such observations are few is that flux jumps in bulk superconductors are often complete, or almost complete. This means that the temperature rises close to T_c in the entire sample, leading to a uniform flux distribution which erases any trace of a possible non-uniformity in the first stages of the flux jump. That contrasts the behavior in thin film samples, where the jumps are usually much smaller and far from being complete.²⁷ This makes non-uniform jumps easier observable in films.^{8–18} Moreover, huge stresses usually exist between a superconducting film and substrate. Abrupt relaxation of these stresses can lead to fluctuations in E , especially for Nb_3Sn or MgB_2 where the superconducting properties depend strongly on the strain.^{2,29} Note also that in films it is much more probable that any perturbation of electric field will influence the whole thickness, whereas it will affect only a small part of a bulk sample. Although our equations for a slab cannot be directly applied to the case of a thin film, we expect that essentially the same physics describes the formation of finger structures in the films too.²⁸ Moreover, non-locality of the current-field relations in films can make formation of non-uniform structures there even more favorable, and possibly account for the branching flux patterns observed experimentally.

The presence of a background electric field \mathbf{E} , and hence moving magnetic flux implies that the background state itself is not stationary. In a typical experiment, the applied magnetic field is increasing $H = H(t)$, the flux front is moving into the sample, $l = l(t)$, and hence the electric field is non-stationary within the flux-penetrated

region. Obviously, our analytical results are valid only if all these quantities change in time slower than the perturbations $\delta\mathbf{E}, \delta T$ grow, i. e., when $\dot{E}/E, \dot{H}/H, \dot{l}/l \ll \lambda$. If the electric field is created by ramping the external magnetic field, $\mathbf{E}(x, t) \simeq \mu_0 \dot{H}[l(t) - x]$, then $\dot{E}/E \approx \dot{H}/H \approx \dot{l}/l$. Using that $\lambda \sim 1/t_0$, we can rewrite the above inequality as $H \gg H_{\text{adiab}}/\sqrt{n}$. Since $n \gg 1$ this condition is satisfied in the major part of the phase diagram in Fig. 6.

In conclusion, a linear analysis of heat diffusion and Maxwell equations shows that a thermomagnetic instability may result in finger-like distributions of T, E and B . The fingering instability arises if the background electric field is so high that the magnetic flux diffusion proceeds much faster than the heat diffusion. Numerical simulations have shown that upon further development of the instability one finger starts growing much faster than the others, and propagates into the flux-free region.

Acknowledgments

This work is supported by INTAS grant 01–2282, NATO Collaborative Linkage Grant 980307 and FUNMAT@UiO. We are thankful for helpful discussions with B. Shapiro, V. Vinokur, P. Leiderer and L. M. Fisher. The work in Houston is supported in part by the State of Texas through the Texas Center for Superconductivity and Advanced Materials at the University of Houston.

* Email for correspondence: t.h.johansen@fys.uio.no

¹ R. G. Mints and A. L. Rakhmanov, *Rev. Mod. Phys.* **53**, 551 (1981).
² A. V. Gurevich, R. G. Mints and A. L. Rakhmanov, *The Physics of Composite Superconductors*, Begell House Inc., NY (1997).
³ S. L. Wipf, *Cryogenics* **31**, 936 (1991).
⁴ Martin N. Wilson, *Superconducting magnets*, Clarendon Press, Oxford, 1983.
⁵ S. L. Wipf, *Phys. Rev. B* **161**, 404 (1967).
⁶ P. S. Swartz and C. P. Bean, *J. Appl. Phys.* **39**, 4991 (1968).
⁷ M. R. Wertheimer and J de G. Gilchrist, *J. Phys. Chem Solids* **28**, 2509 (1967).
⁸ P. Leiderer, J. Boneberg, P. Brüll, V. Bujok, S. Herminghaus, *Phys. Rev. Lett.* **71**, 2646 (1993).
⁹ U. Bolz, J. Eisenmenger, J. Schiessling, B.-U. Runge, P. Leiderer, *Physica B* **284-288**, 757 (2000).
¹⁰ U. Bolz, D. Schmidt, B. Biehler, B.-U. Runge, R. G. Mints, K. Numssen, H. Kinder, P. Leiderer, *Physica C* **388-389**, 715 (2003).
¹¹ C. A. Duran, P. L. Gammel, R. E. Miller, D. J. Bishop, *Phys. Rev. B* **52**, 75 (1995).
¹² V. Vlasko-Vlasov, U. Welp, V. Metlushko, G. W. Crabtree,

Physica C **341-348**, 1281 (2000).

¹³ T.H. Johansen, M. Baziljevich, D.V. Shantsev, P.E. Goa, Y.M. Galperin, W.N. Kang, H.J. Kim, E.M. Choi, M.-S. Kim, S.I. Lee, *Europhys. Lett.* **59**, 599 (2002). cond-mat/0104113
¹⁴ T.H. Johansen, M. Baziljevich, D.V. Shantsev, P.E. Goa, Y.M. Galperin, W.N. Kang, H.J. Kim, E.M. Choi, M.-S. Kim, S.I. Lee, *Supercond. Sci. Technol.* **14**, 726 (2001). cond-mat/0108092.
¹⁵ A.V. Bobyl, D.V. Shantsev, T.H. Johansen, W.N. Kang, H.J. Kim, E.M. Choi, S.I. Lee, *Appl. Phys. Lett.* **80**, 4588 (2002), cond-mat/0201260.
¹⁶ F. L. Barkov, D. V. Shantsev, T. H. Johansen, P. E. Goa, W. N. Kang, H. J. Kim, E. M. Choi, S. I. Lee, *Phys. Rev. B* **67**, 064513 (2003). cond-mat/0205361.
¹⁷ A. V. Bobyl et al. *Physica C*, in press, cond-mat/0304603.
¹⁸ I.A. Rudnev, S.V. Antonenko, D.V. Shantsev, T.H. Johansen, A.E. Primenko, *Cryogenics* **43**, 663 (2003). cond-mat/0211349
¹⁹ I. Aranson, A. Gurevich and V. Vinocur, *Phys. Rev. Lett.* **87**, 067003 (2001).
²⁰ B. Shapiro et al., submitted to *Phys. Rev. B*
²¹ R. G. Mints, A. L. Rakhmanov, *J. Phys. D: Appl. Phys.* **9**, 2281 (1976).

- ²² Most curves in Fig. 3 show a kink when the discriminant of Eq. (20) changes sign, which marks appearance of a non-zero $\text{Im } \lambda$.
- ²³ Y.-B. Kim, C. F. Hempstead, and A. R. Strnad, Phys. Rev. **129**, 528 (1963)
- ²⁴ M. Sander, U. Sutter, M. Adam and M. Klaser, Supercond. Sci. Technol. **15** (2002) 748.
- ²⁵ A. B. Surzhenko, S. Schauroth, D. Litzkendorf, M. Zeisberger, T. Habisreuther and W. Gawalek, Supercond. Sci. Technol. **14** (2001) 770.
- ²⁶ E. Altshuler and T. H. Johansen, Rev. Mod. Phys. **76**, 471 (2004), cond-mat/0402097.
- ²⁷ Z. W. Zhao, S. L. Li, Y. M. Ni, H. P. Yang, Z. Y. Liu, H. H. Wen, W. N. Kang, H. J. Kim, E. M. Choi, and S. I. Lee, Phys. Rev. B **65**, 064512 (2002).
- ²⁸ Similar results for films have recently been reported by I. S. Aranson *et al.*, cond-mat/0407490.
- ²⁹ C. Buzea and T. Yamashita, Supercond. Sci. Technol. **14**, R155 (2001).